International Journal of Pharmaceutics: X 1 (2019) 100027

Contents lists available at ScienceDirect

International Journal of Pharmaceutics: X

journal homepage: www.journals.elsevier.com/international-journal-of-pharmaceutics-x

Mechanism investigation of ethosomes transdermal permeation

Xiao-Qian Niu[a,b], Dan-Ping Zhang[a], Qiong Bian[a], Xing-Fu Feng[c], Hao Li[d], Yue-Feng Rao[e,*], Yong-Mei Shen[f], Fu-Neng Geng[f], An-Ran Yuan[a], Xiao-Ying Ying[a], Jian-Qing Gao[a,b,*]

[a] Institute of Pharmaceutics, College of Pharmaceutical Sciences, Zhejiang University, Hangzhou 310058, PR China
[b] Jiangsu Engineering Research Center for New-Type External and Transdermal Preparations, PR China
[c] Ningbo Saiyusi Biotechnology Co., Ltd., Ningbo 315806, PR China
[d] Sanova Bioscience Inc., 42 Nagog Park, STE110, Acton, MA 01741, USA
[e] Department of Pharmacy, The First Affiliated Hospital, School of Medicine, Zhejiang University, Hangzhou 310058, PR China
[f] Sichuan Gooddoctor Pharmaceutical Group Co., Ltd, Chengdu 610000, PR China

ARTICLE INFO

Keywords:
Ethosomes
Skin
Transdermal delivery
Mechanism
Lipid

ABSTRACT

Ethosomes are widely used to promote transdermal permeation of both lipophilic and hydrophilic drugs, but the mechanism of interaction between the ethosomes and the skin remains unclear. In this work, it was exploded with several technologies and facilities. Firstly, physical techniques such as attenuated total reflectance fourier-transform infrared and laser confocal Raman were used and the results indicated that the phospholipids configuration of stratum corneum changes from steady state to unstable state with the treatment of ethosomes. Differential scanning calorimetry reflected the thermodynamics change in stratum corneum after treatment with ethosomes. The results revealed that the skin of Bama mini-pigs, which is similar to human skin, treated by ethosomes had a relatively low T_m and enthalpy. Scanning electron microscopy and transmission electron microscopy showed that the microstructure and ultrastructure of stratum corneum was not damaged by ethosomes treatment. Furthermore, confocal laser scanning microscopy revealed that lipid labeled ethosomes could penetrate the skin via stratum corneum mainly through intercellular route, while during the process of penetration, phospholipids were retained in the upper epidermis. Cell experiments confirmed that ethosomes were distributed mainly on the cell membrane. Further study showed that only the drug-loaded ethosomes increased the amount of permeated drug. The current study, for the first time, elucidated the mechanistic behavior of ethosomes in transdermal application from molecular configuration, thermodynamic properties, ultrastructure, fluorescent labeling and cellular study. It is anticipated that the approaches and results described in the present study will benefit for better design of drug-loaded ethosomes.

1. Introduction

The body's skin barrier against influences from the environment is essentially formed by its uppermost layer, the stratum corneum (SC). The SC is the final product of epidermal differentiation with approximately 10–20 μm thickness and is metabolically inactive (Oh et al., 2002). It is comprised of 10–25 layers of dead, elongated, fully keratinized corneocytes, which are embedded in a matrix of the lipid bilayers. This structure is called "Brick and Mortar" type structure (Polat et al., 2012). The extracellular lipid is constituted of predominant crystalline phase and the subpopulation of liquid lipid phase (Bouwstra and Ponec, 2006). When applying substances onto the skin in order to reach the underlying viable epidermis, these substances always have to pass the SC lipid regions. Consequently, the lipid matrix provides the main barrier of the skin.

Lipid dosage forms for transdermal delivery are mainly liposomes and its derivatives such as transfersomes, niosomes and ethosomes. The transfersomes and niosomes are mainly transported in the pores between keratinocytes and the liposomes are mainly transported through hair follicles (Abd El-Alim et al., 2019; Yang et al., 2019). As a lipid vehicle, ethosomes have shown superb effectiveness in percutaneous drug delivery. In addition, they have superior pharmaceutical properties, including stability at room temperature, high entrapment efficiency, and improved compatibility with the SC, thus promoting the penetration of both hydrophilic and lipophilic drugs through the stratum corneum (SC) into the deep layers of the skin more effectively

* Corresponding authors at: Institute of Pharmaceutics, College of Pharmaceutical Sciences, Zhejiang University, 866 Yuhangtang Road, Hangzhou 310058, Zhejiang, PR China (J. Gao).
E-mail addresses: raoyf@zju.edu.cn (Y.-F. Rao), gaojianqing@zju.edu.cn (J.-Q. Gao).

https://doi.org/10.1016/j.ijpx.2019.100027
Received 5 May 2019; Received in revised form 16 July 2019; Accepted 4 August 2019
Available online 07 August 2019

than traditional liposomes (Touitou et al., 2000; Yu et al., 2015). Given that many studies using ethosomes to promote drug penetration, and ethosomes contain higher concentrations of ethanol and lipids (Goindi et al., 2014), it is important to understand its effects on the skin. It was reported that the presence of ethanol in the formulation allowed drug solubilization and created deformable lipid structures that could easily pass between skin corneocytes, resulting in drug skin retention and permeation enhancement (Marto et al., 2016; Roberts et al., 2017). However, the mechanism of transdermal permeation promotion by ethosomes and the impact on skin is not well understood (Chen et al., 2017; Limsuwan et al., 2017; Yang et al., 2017).

At present, the main techniques to study the transdermal mechanism include Attenuated Total Reflectance Fourier Transform Infrared Spectroscopy (ATR-FTIR) (Wang et al., 2018), Confocal Laser Scanning Microscopy (CLSM) (Zhao et al., 2017), Differential Scanning Calorimeter (DSC) (Liu et al., 2017), Raman (Melot et al., 2009), Scanning Electronic Microscopy (SEM) (Park et al., 2018), Transmission Electron Microscope (TEM) (Yin et al., 2017), X-ray Photoelectron Spectroscopy (XPS) (Mandal et al., 2017) and Electron Spin Resonance (ESR) (Moll et al., 2008). These techniques have facilitated the research on transdermal mechanism. However, these techniques have not been extensively used for the study of the transdermal mechanism of ethosomes, except fluorescent labeling and ATR-FTIR (Ashtikar et al., 2016; Brewer et al., 2013; Cevc and Vierl, 2010). Drawing on the methods in other transdermal mechanisms research and our previous study (Li et al., 2014; Rao et al., 2008), the transdermal mechanism of ethosomes was tried to elucidate from molecular configuration, thermodynamic properties, ultrastructure, fluorescent labeling, and cellular levels for the first time. The techniques used are ATR–FTIR, DSC, Raman SEM and TEM.

Furthermore, ATR–FTIR and laser confocal Raman are used to detect molecular configuration change in the skin. ATR–FTIR and laser confocal Raman, as complementary detection means, provide more detailed information on the lateral organization and the conformational ordering in the lipid phases. DSC, as one of thermal analysis methods, is widely used for characterization of the melting of lipids, the phase transition of lipid bilayers and protein denaturation in SC layer. By comparing mean transition temperature (T_m) and enthalpies ($\triangle H$), thermotropic behavior of treated skin is assessed. SEM and TEM show the microstructure and ultrastructure change of SC. SEM has a large depth of field compared with conventional light microscopy and for that reason the images obtained have a three-dimensional appearance, high resolution at high magnifications, revealing details of the skin surface. TEM is the most efficient way to visualize the ultrastructure of the SC. Furthermore, by CLSM, the percutaneous pathway and distribution of ethosomes are visualized. To accurately understand the contact between skin cells and ethosomes, we also study at the cellular level.

In this study, the ethosomes-encapsulated drug is Donepezil HCL (DPH). As one of reversible acetylcholinesterase inhibitor, DPH is currently the most prescribed pharmacological agent for the treatment of Alzheimer's disease (Schmidt et al., 2015). DPH is superior to other acetylcholinesterase inhibitors due to its high potency and selectivity for the enzyme in the central nervous system (Lam and Gambari, 2014). Since DPH also causes gastrointestinal adverse effects, a transdermal delivery system may avoid gastrointestinal adverse effects and work as a suitable method to overcome the problems of conventional oral administration of DPH.

This present study uses various techniques means to study the transdermal mechanism of ethosomes (Fig. 1), and try to describe the transdermal mechanistic behavior of ethosomes.

2. Materials and methods

2.1. Materials

The compound 1-palmitoyl-2-{12-[(7-nitro-2–1,3-benzoxadiazol-4-yl)amino] dodecanoyl}-sn-glycero-3-phosphocholine (NBD-PC) was purchased from Avanti Polar Lipids (Alabaster, AL, USA). Rhodamine B (RhB) was purchased from Sigma-Aldrich (Missouri, USA). LIPOID S PC (PC) (phosphatidylcholine content 70%) was purchased from Lipoid Gmbh (Ludwigshafen, Germany). Ethanol dimethyl sulfoxide (DMSO) were purchased from Aladdin (Shanghai, China). Celltracker CM-DiI (CM-Dil) was purchased from YEASEN (Shanghai, China). Human adult low calcium high temperature (HaCaT) cell line was purchased from Kunming Cell Bank of Chinese Academy of Science (Kunming, China). Bama miniature pig was purchased from Shanghai Jiagan Biological Technology Co., Ltd (Shanghai, China). Newborn calf serum was purchased from Gibco BRL (Gaithersburg, MD, USA). Donepezil HCL was a gift from Zhejiang Huahai Pharmaceutical Co., Ltd. (Linhai, China). Milli-Q water was used throughout the experiment. All chemicals were used as received without any modification.

2.2. Preparation of ethosomes

The ethosomes were prepared by ethanol injection. First, 40 mg of DPH and 40 mg of PC were dissolved in 0.6 mL of ethanol, and the ethanol solution was injected into a 1.4 mL phosphate buffer solution (pH 6.8) at a rate of 200 μL/min under closed conditions. After the ethanol solution was added, stired for 10 min. The prepared ethosomes was ultrasonicated for 2 min and the ultrasound power was 35% (the total rated power is 650 W). Then passed through a 0.22 μm filter for three times (Fan et al., 2013).

2.3. Preparation of fluorescence labeling ethosomes

2.3.1. NBD-PC labeled ethosomes

The NBD-PC labeled ethosomes were prepared by ethanol injection. First, 40 mg of DPH, 40 mg of PC and 0.01% NPC-PC were dissolved in 0.6 mL of ethanol. The following preparation method of fluorescence labeling ethosomes reference part 2.2.

2.3.2. NBD-PC and RhB labeled ethosomes

The ethosomes were prepared by ethanol injection. First, 40 mg of DPH, 40 mg of PC, 0.01% NPC-PC, 0.03% RhB were dissolved in 0.6 mL of ethanol. The following preparation method of fluorescence labeling ethosomes reference part 2.2.

2.4. Characterization of ethosomes-particle size, polydispersity index (PDI), zeta potential and TEM

Particle size, PDI, and zeta potential of the optimal DPH ethosomes were analyzed by Malvern Zetasizer Nano ZSP (Malvern Instruments Inc., Malvern, UK). Temperature and scattering angle were set at 25 °C ± 1 °C and 90°. The sample was not diluted and used directly to determine the average size, PDI, and average zeta potential.

The morphology of ethosomes was characterized by TEM (Tecnai G2 spirit, Thermo FEI, America). One drop of each ethosomes vesicle preparation was placed onto a copper grid, and the excess suspension was immediately adsorbed using filter paper. The sample was then negatively stained by adding a drop of 2% phosphotungstic acid, followed by drying at room temperature. Afterward, the grid was observed using a TEM with an accelerating voltage of 120 kV.

2.5. Entrapment efficiency of DPH-loaded ethosomes

The entrapment efficiency of the DPH-loaded ethosomes was determined using dialysis centrifugation method (Zhang et al., 2014).

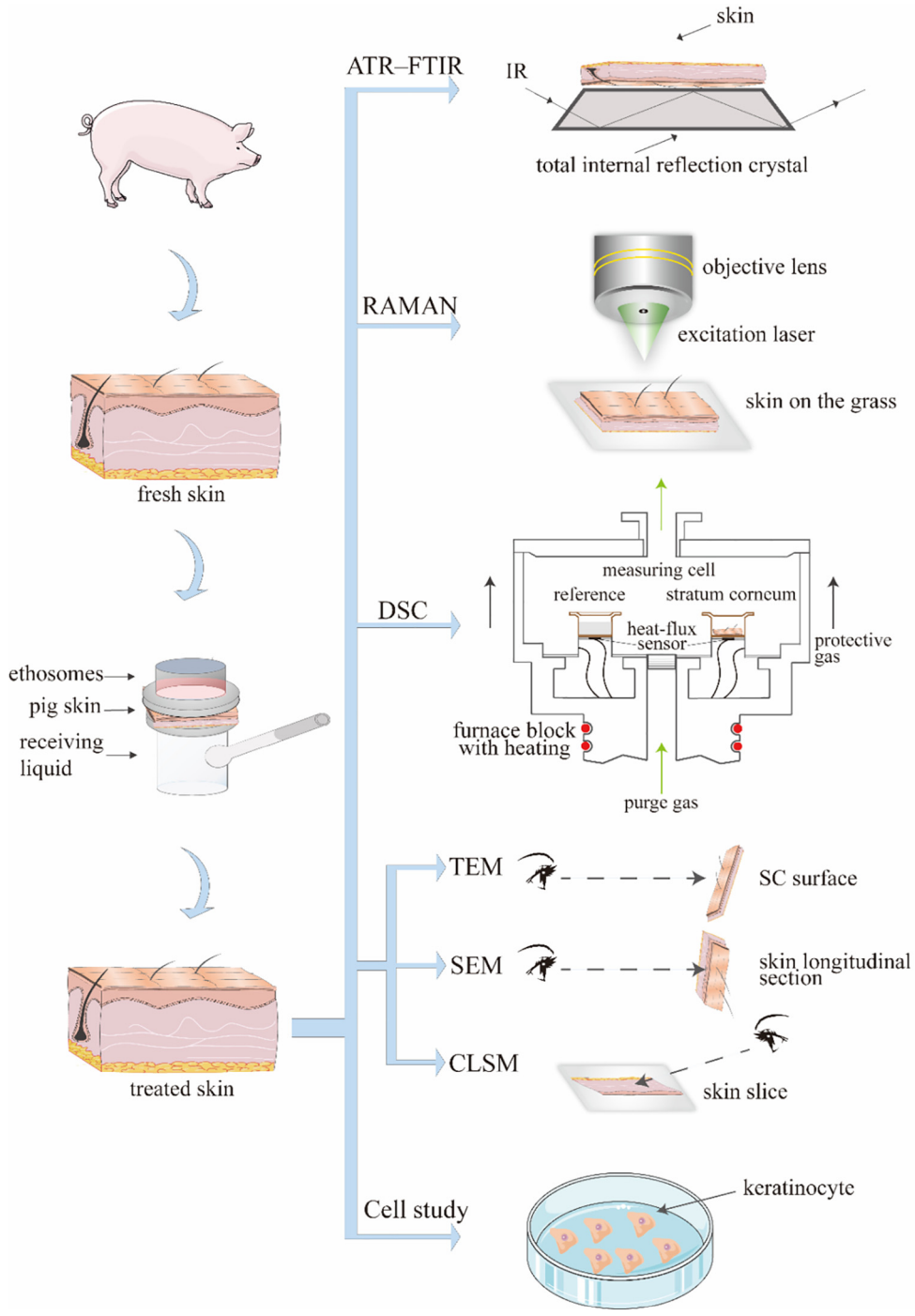

Fig 1. The framework of research thoughts.

Briefly, 1 mL DPH-loaded ethosomes was placed into a dialysis bag (molecular weight cutoff [MWCO] 8000–14,000 Da) and two ends of the dialysis bag were tied (n = 3). This dialysis bag was then put into the 10 mL centrifuge tube which was filled with 7 mL receptor phase (a mixture of ethanol and water at 1:1 ratio) and centrifuged for an hour at 6000 rpm. The DPH content in the receptor phase was further estimated by high performance liquid chromatography (HPLC). The conditions of the HPLC method (Saluja et al., 2013) were as follows: mobile phase was composed of methanol and aqueous solution of 0.1% trifluoroacetic acid (40:60); injection volume 10 μL; detection wavelength 270 nm; column: waters exterra MS C_{18} (5 μm, 4.6 × 150 mm); column temperature 40 °C, and flow rate 1.0 mL/min. The total drug contained in the DPH-loaded ethosomes was determined by disrupting the mixture with methanol. The entrapment efficiency was calculated using the following equation: entrapment efficiency % = $(1 - W_{free\ drug}/W_{total\ drug}) \times 100\%$.

2.6. Transdermal experiment

Bama-type pigs (weighing ~2.5 kg) were purchased from Shanghai Jiagan Biological Technology Co., Ltd. (Shanghai, China). All procedures performed were in accordance with Zhejiang University's guidelines for welfare of experimental animals. The study was approved by the animal ethics committee of Zhejiang University. The skin used was 2.5 kg Bama-type pig's back and part of the abdomen skin. The full thickness pig skin was dermatomed to a thickness of 1.2 mm by Padgett-

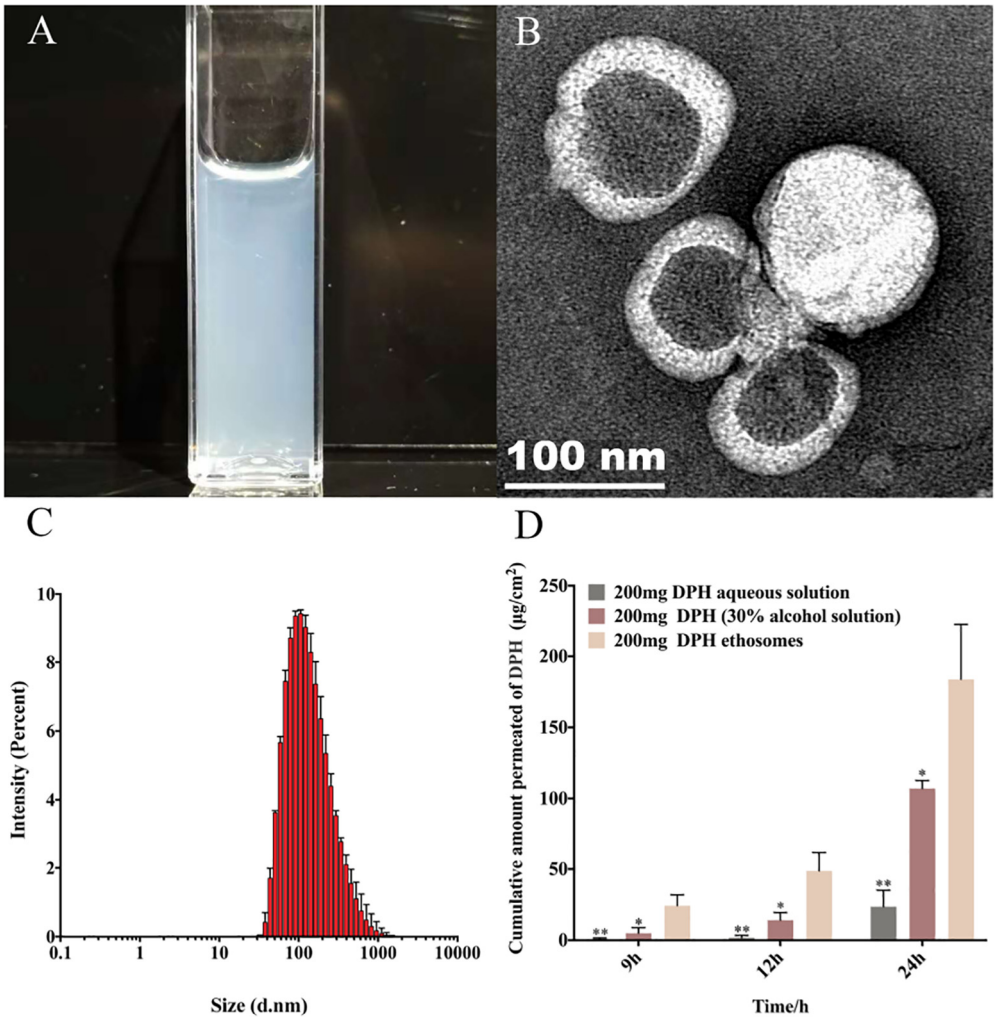

Fig 2. Characterization of ethosomes. (A) appearance characteristics. (B) TEM of ethosomes. (C) size distribution (D) transdermal effect of different DPH formulations, n = 3, * denotes statistical significance at a level of $p < 0.05$; ** denotes statistical significance at a level of $p < 0.01$ with DPH aqueous solution).

Table 1
Characterization of the DPH-loaded exosomes (n = 3).

Particle size (nm)	Polydispersity index	Zeta potential (mV)	Encapsulated efficiency (%)
120.7	0.244	25.8	78.21 ± 0.37

Hood dermatome (Shanghai Yuanxing Medical Device Manufacturing Co., Ltd, China) and then stored frozen at −80 °C for further use. When used, the frozen skin was placed in PBS for 30 min and then placed on a transdermal diffusion cell, which covered 3.14 cm^2. Transdermal receptor was saline. Different groups were added to the top of the transdermal diffusion cell. Control group was PBS and the experimental groups were 20 mg/ml DPH water solution, 30% ethanol-20 mg/ml DPH solution and 20 mg/ml DPH ethosomes (n = 3).

The transdermal receiving solution was taken at 3 h, 6 h, 9 h, 12 h, 24 h and centrifugated at 15,000 rpm for 10 min. Then the supernatant was taken for detection by HPLC which referred to part 2.5. Take 1 mL of transdermal receptor solution at each time point and replenish fresh receiving solution 1 mL. Formula for calculating the cumulative amount permeated of DPH:

$$Q = \frac{C_n \times V + \sum C_{n-1} \times 1}{3.14}$$

In the formula, Q: cumulative transdermal amount per unit area; V: receiving liquid volume; C_n: concentration of the sampling.

The equation obtained by linear regression with Q as the ordinate and time T as the abscissa is the Higuchi equation, and the slope is the transdermal rate constant J (μg/cm^2/h). The multiplication factor Er = J/J_0 (J_0: permeation rate of the percutaneous absorption enhancer), the permeability coefficient Pm ($cm \cdot h^{-1}$) = J/C_0 (C_0: initial concentration of the drug in the diffusion cell, μg/mL).

2.7. Attenuated total reflectance fourier-transform infrared (ATR–FTIR)

Skin samples with a dimension of about 3.14 cm^2 (ZnSe crystal dimension) were adopted for the experiment.

The following formulation groups were used (n = 3):

(1) Application of 2 mL PBS (control) for 24 h
(2) Application of 2 mL 20 mg/ml DPH water solution for 24 h
(3) 30% ethanol-20 mg/ml DPH solution for 24 h (the ethanol concentration is same as ethosomes)
(4) 3 mg/ml DPH ethosomes for 24 h.

All formulations were prepared as previously described. The penetration depth of IR was about 1 μm or less, which included approximately 1–1.5 sheets of cell layers in the SC. Infrared spectra of the prepared skin samples were obtained by using FTIR spectrophotometer (NICOTCT, America). To collect the spectra, the skin samples were

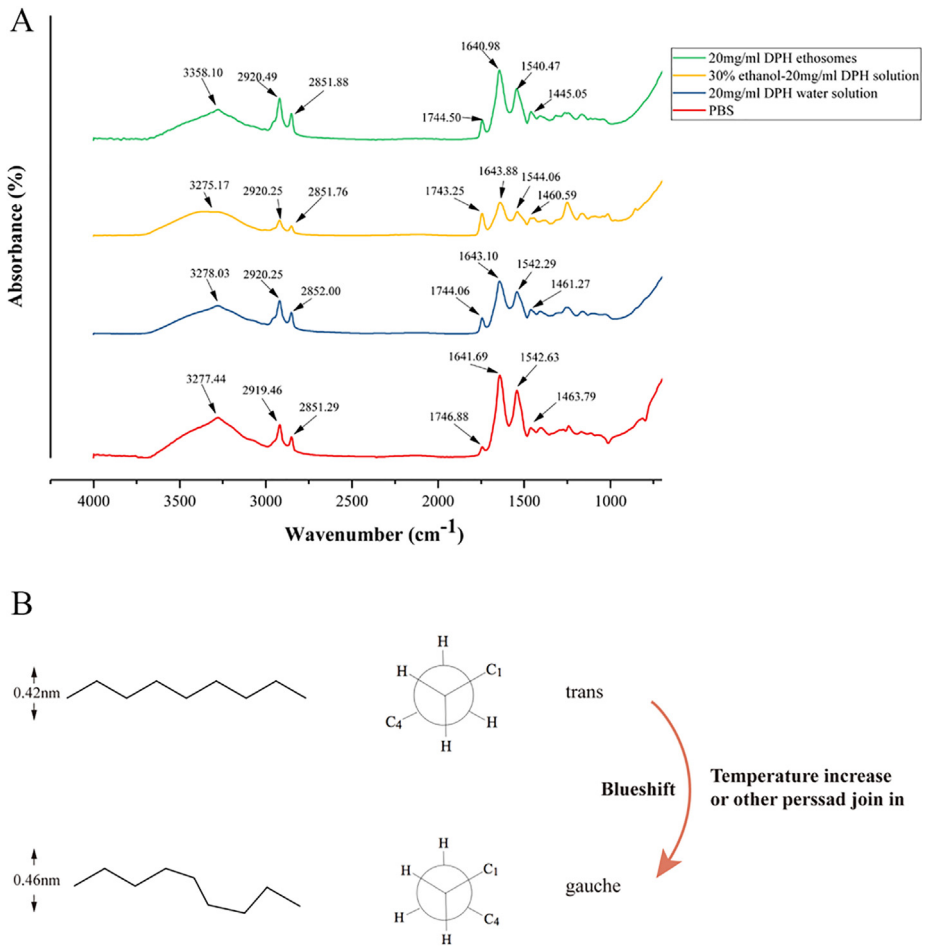

Fig 3. (A) Comparison of FTIR transmission spectra of application different formulations on pig skin. (B) Mechanism of molecular configuration change.

Table 2
FT-IR C—H wave numbers (cm^{-1}) changes compared with control and abdominal hydrated whole pig skin following treatment with different vehicles. (Each value represents the mean ± S.D. n = 3, * denotes statistical significance at a level of $p < 0.05$; ** denotes statistical significance at a level of $p < 0.01$ with PBS control group).

Group	CH_2 sym stretching		CH_2 asym stretching		CH_2 scissoring
	wavenumber/cm^{-1}	height	wavenumber/cm^{-1}	height	width
PBS	2851.50 ± 0.41	0.09 ± 0.02	2919.19 ± 0.24	0.14 ± 0.02	56.57 ± 2.13
20 mg/ml DPH water solution	2851.96 ± 0.21	0.10 ± 0.02	2919.82 ± 0.58	014 ± 0.04	56.57 ± 2.13
30% ethanol −20 mg/ml DPH solution	2851.46 ± 0.27	0.05 ± 0.01*	2919.70 ± 0.48	0.09 ± 0.01*	55.28 ± 2.13
20 mg/ml DPH ethosomes	2852.56 ± 0.46*	0.05 ± 0.01*	2920.96 ± 0.77*	0.09 ± 0.02*	66.85 ± 2.13*

placed SC down onto the ZnSe ATR crystal. Software OMNIC 9.2 was used to analysis the data.

3.1. Laser confocal Raman

Raman spectral acquisitions were performed with an HR Labram microspectrometer (LabRAM HRevolution, France). The excitation source was a 633-nm single-mode diode laser generating 17 mW on the sample 633 nm. For the study, the selected spectral range was selected from 900 to 1800 cm^{-1} and from 2700 to 3100 cm^{-1}. Each single spectrum was recorded using a 50 × objective (a high stability study stage microscope), an exposure time of 2 s, and 18 accumulations was at each spot. Spectral acquisition was performed using Labspec6 software (Horiba Jobin Yvon SAS, France). Skin samples adopted for the experiment refer to 2.7.

3.2. DSC of skin

For DSC, approximately 5–10 mg of SC sheets (treated or untreated) were cut in form of disks and placed in 40 μL aluminum standard pans. Skin samples adopted for the experiment refer to 2.7. Thermal analysis was performed using a STARe/Thermal Analysis System (Mettler-Toledo, Switzerland, DSC 1). All samples were analyzed between 20 and 200 °C at 10 °C/min heating rate under nitrogen flow. The transition temperature (T_m) and their corresponding enthalpies were noted and results were evaluated statistically using TTest through Origin software (State College, PA).

3.3. SEM of skin

Skin samples adopted for the experiment refer to 2.7. After treated by different formulations for 24 h, the skin samples were treated as

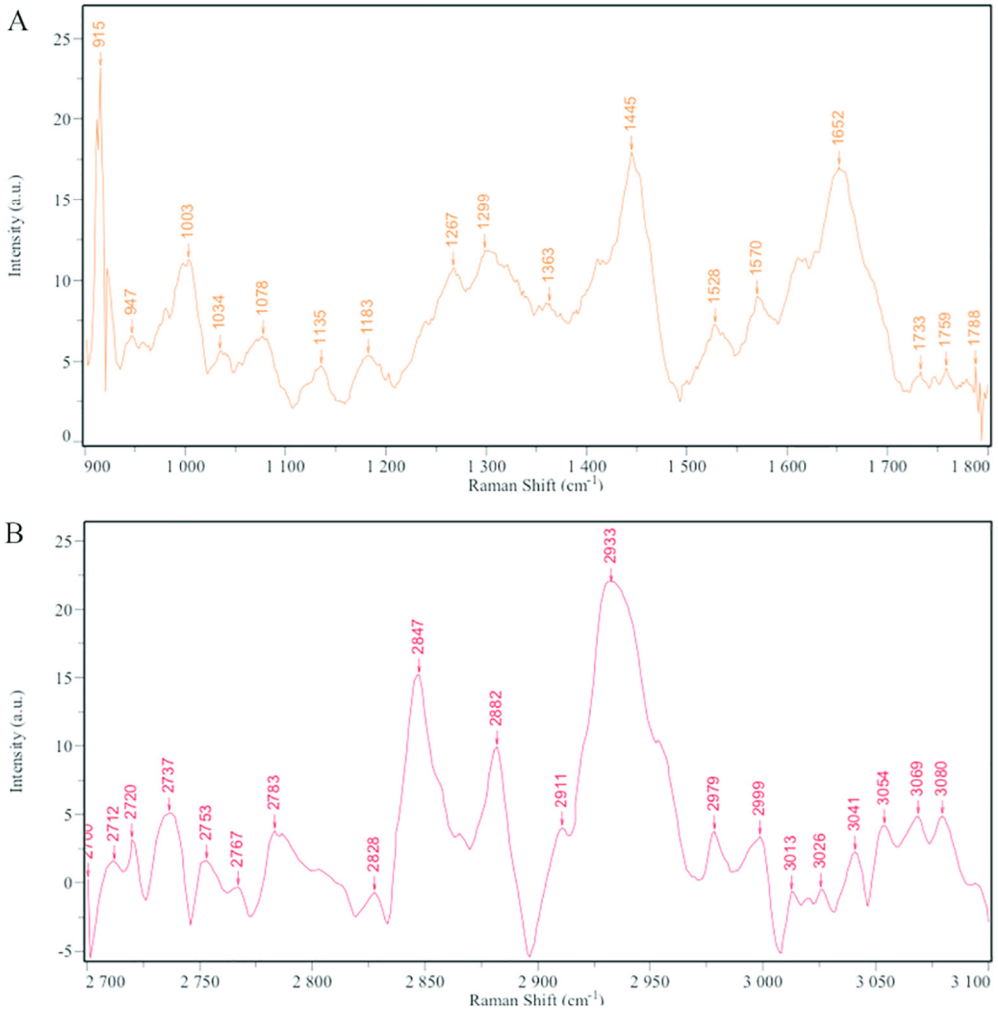

Fig. 4. Raman spectra of skin. (A) in the 900–1800 cm^{-1} region; (B) in the 2700–3100 cm^{-1} region).

follows:

Double fixation: The samples were cut into 1 cm × 1 cm size and first fixed with 2.5% glutaraldhyde in phosphate buffer (0.1 M, pH7.0) for more than 4 h; washed three times in the phosphate buffer (0.1 M, pH7.0) for 15 min at each step; then postfixed with 1% O_SO_4 in phosphate buffer for 1–2 h and washed three times in the phosphate buffer (0.1 M, pH7.0) for 15 min at each step. Next, dehydration: the sample was first dehydrated by a graded series of ethanol (30%,50%,70%,80%,90%,95% and 100%) for about 15 to 20 min at each step, transferred to the mixture of ethanol and iso-amyl acetate (v:v = 1:1) for about 30 min, then transferred to pure iso-amyl acetate for about 1 h or overnight. In the end, the sample was dehydrated in Hitachi Model HCP-2 critical point dryer with liquid CO_2. Finally, coating and observation: the dehydrated sample was coated with gold-palladium in Hitachi Model E-1010 ion sputter for 4–5 min and observed in Hitachi Model TM-1000 SEM.

3.4. TEM of skin

Skin samples adopted for the experiment refer to 2.7. After treated by different formulations for 24 h, the skin samples were treated as follows:

First, double fixation: the specimen was first fixed with 2.5% glutaraldehyde in phosphate buffer (pH7.0) for more than 4 h; washed three times in the phosphate buffer; then postfixed with 1% OsO_4 in phosphate buffer (pH7.0) for 1 h and washed three times in the phosphate buffer. Then, dehydration: the specimen was first dehydrated by a graded series of ethanol (30%, 50%, 70%, 80%, 90%, 95% and 100%) for about 15 to 20 min at each step, transferred to absolute acetone for 20 min. Next, infiltration: the specimen was placed in 1:1 mixture of absolute acetone and the final Spurr resin mixture for 1 h at room temperature, then transferred to 1:3 mixture of absolute acetone and the final resin mixture for 3 h and to final Spurr resin mixture for overnight. Finally, embedding and ultrathin sectioning: specimen was placed in capsules contained embedding medium and heated at 70 °C for about 9 h. The specimen sections were stained by uranyl acetate and alkaline lead citrate for 15 min respectively and observed in TEM of Model H-7650.

3.5. Laser scanning confocal microscope

The fluorescently labeled ethosomes were applied to transdermal experiments to observe the distribution of fluorescently labeled ethosomes in the skin. After 24 h experiment, the skin tissue samples were washed in PBS for 3 times and then embedded in embedding medium, sectioned at 8 μm thicknesses immediately, with a cryo-ultramicrotome, and observed with CLSM (Zeiss LSM 800), with an excitation wavelength of 488 nm and 552 nm. The blank group ethosomes were used as a control to avoid interference from autofluorescence. All procedures were carried out in the dark to prevent the influence of ambient light. The fluorescence intensity of each image was measured by Zen 2.3 (blue edition) software.

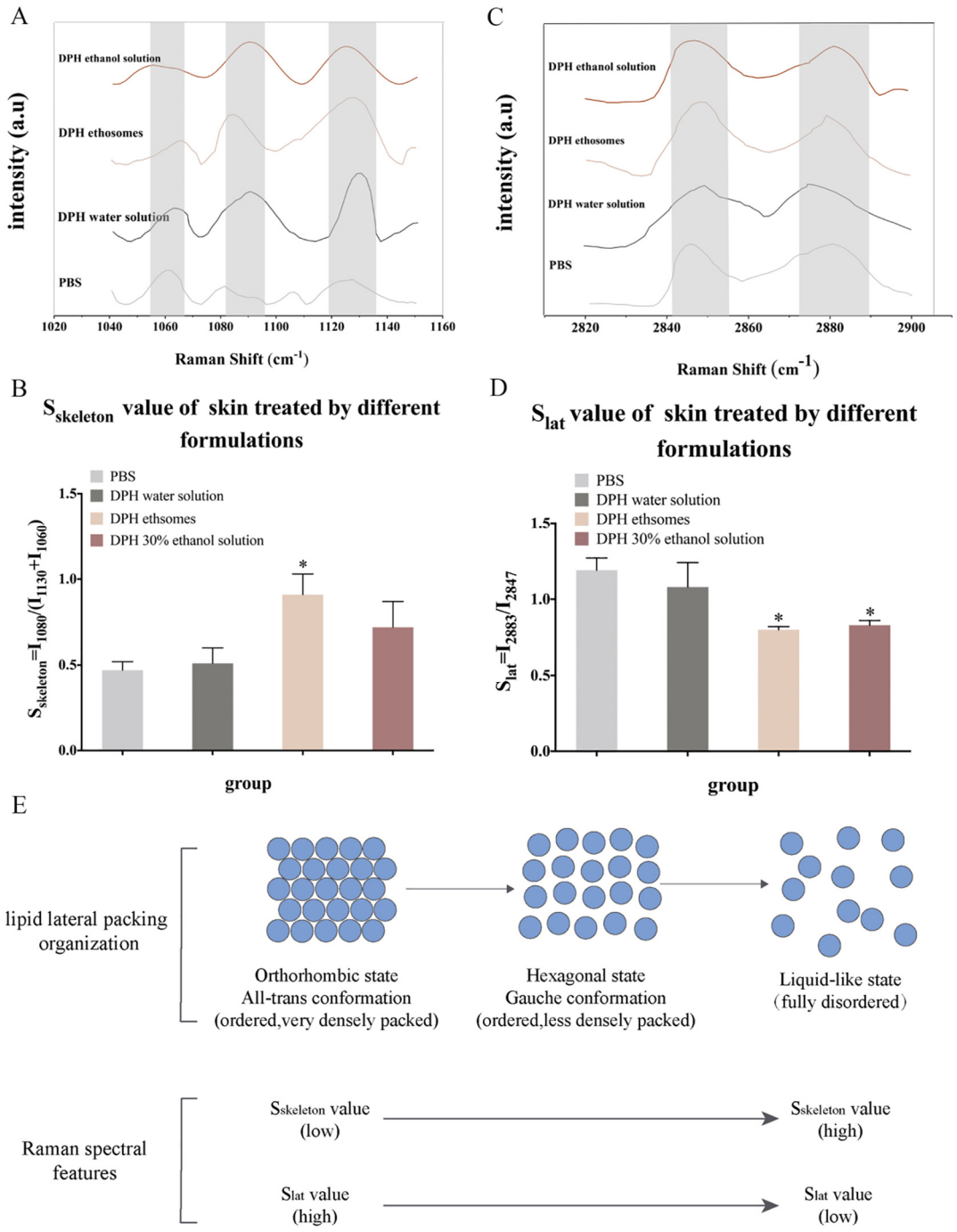

Fig 5. Raman spectra of pig skin. (A) in the 1040–1150 cm^{-1} region. (B) the $S_{skeleton}$ of skin treated by different group. (C) in the 2820–2900 cm^{-1} region. (D) the S_{lat} of skin treated by different group. (E) The relationship between lipid lateral packing organization and Raman spectroscopic features. n = 3, * denotes statistical significance at a level of $p < 0.05$with PBS control group).

3.6. Study on contact between ethosomes and keratinocytes

In order to observe the distribution of ethosomes in keratinocytes, the cellular level was studied. Keratinocytes cell membrane staining: the storage solution was prepared in DMSO at a concentration of 2 mg/mL; the working solution was prepared by diluting the storage solution with D-PBS to prepare a working solution with a concentration of 2 μM; after the iron wall of the cell, the cells were in the dyeing working solution. Incubated at 37 °C for 10 min and then incubated for 10 min at 4 °C; after labeling, the cells were washed by PBS for 3 times.

50 μL of NBD-PC labeled ethosomes were separately added to 1 mL of culture medium, and incubated with the cultured keratinocytes for 3 h, 12 h, and 24 h. Then the cells were washed with PBS for 3 times and fixed by 4% paraformaldehyde for 15 min to observe by CLSM (Zeiss LSM 800). All procedures were carried out in the dark to prevent the influence of ambient light. The fluorescence intensity of each image was measured by Zen 2.3 (blue edition) software.

3.7. Skin recovery performance

In order to study whether pretreatment of skin with blank ethosomes can increase the subsequent percutaneous penetration of DPH, skin recovery performance was tested. PBS and blank ethosomes were added to the top of the transdermal diffusion cell. After 24 h, the PBS

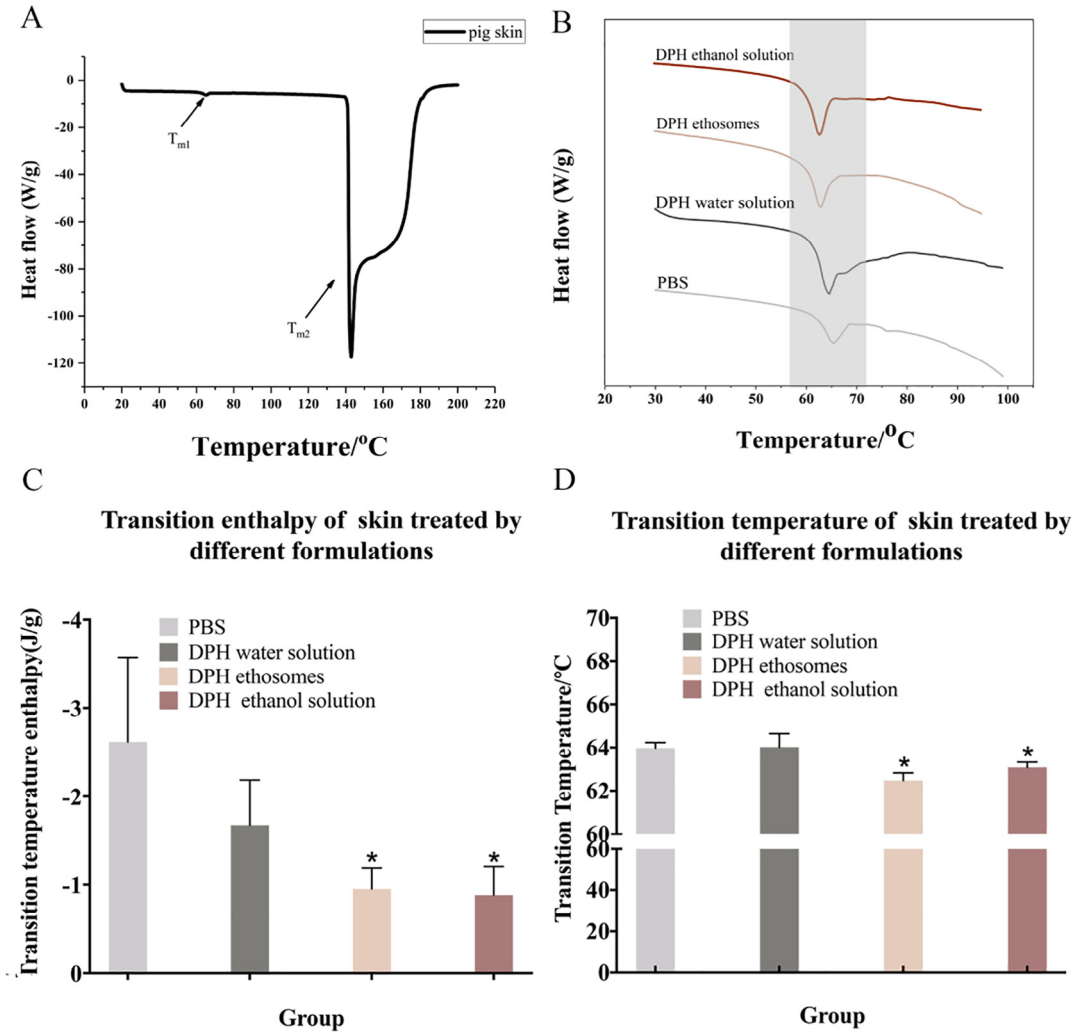

Fig 6. The DSC result of pig SC. (A) the whole DSC curve of pig skin SC. (B) the partial enlarged DSC detail of pig skin treated by different formulations. (C) The mean transition temperature of skin treated by different formulations. (D) The mean transition enthalpy of skin treated by different formulations. n = 3, * denotes statistical significance at a level of $p < 0.05$with PBS control group).

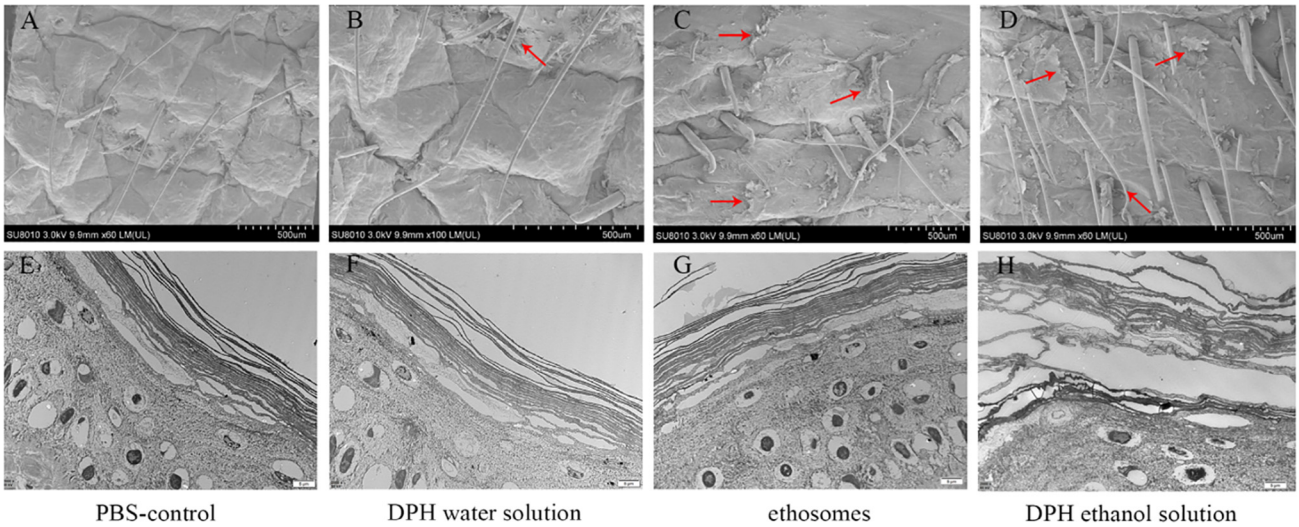

Fig 7. SEM and TEM of different formulations treated skin samples. (A) SEM of skin applicated PBS for 24 h. (B) SEM of skin applicated DPH water solution for 24 h. (C) SEM of skin applicated DPH ethosomes for 24 h. (D) SEM of skin applicated 30% ethanol DPH solution for 24 h.(E) TEM of SC applicated PBS for 24 h. (F) TEM of SC applicated DPH water solution for 24 h. (G) TEM of SC applicated DPH ethosomes for 24 h. (H) TEM of SC applicated 30% ethanol DPH solution for 24 h, the pictures in the same column belong to the same group, red arrow represents SC exfoliation).

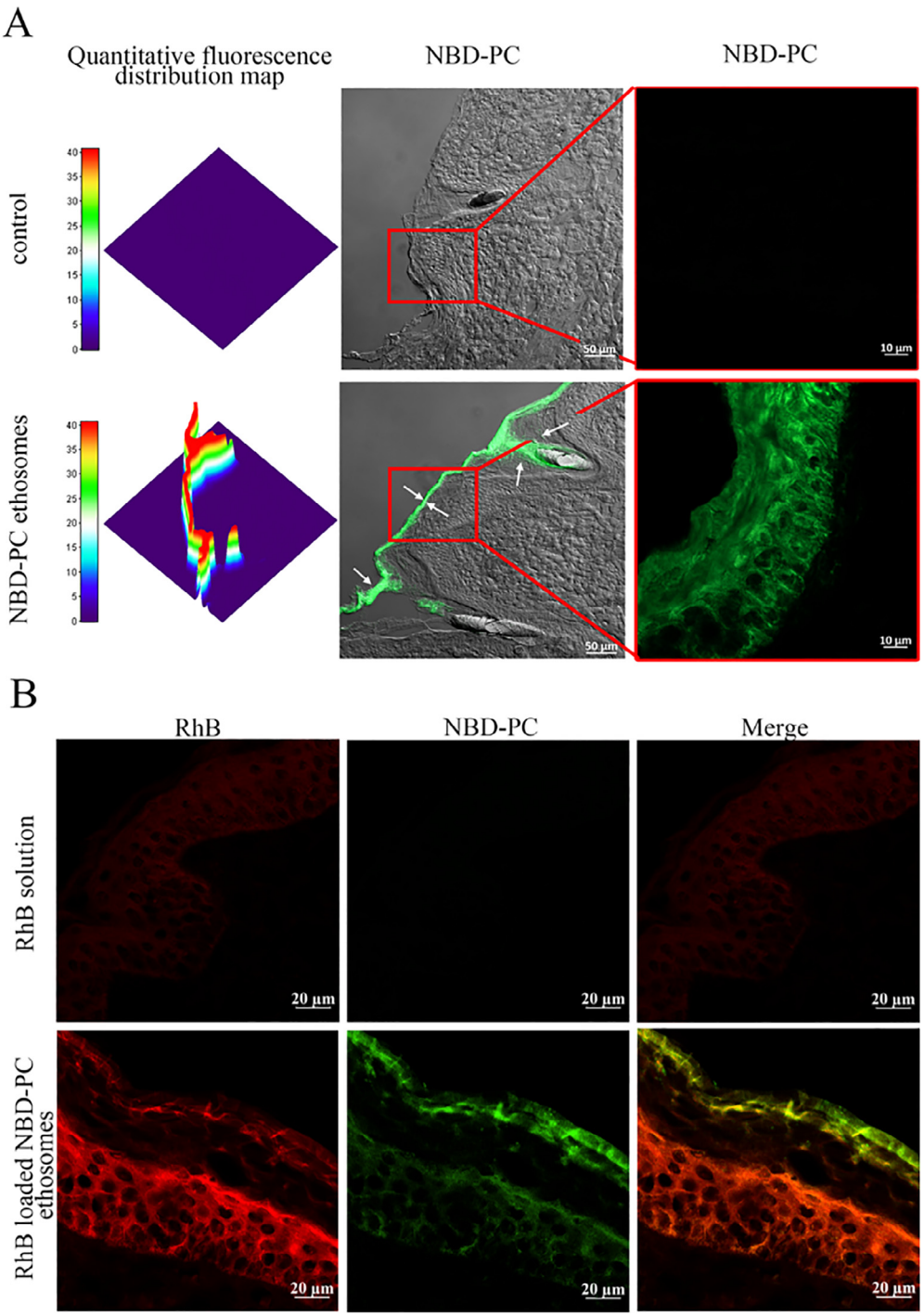

Fig 8. Confocal laser scanning microscopy images of pig skin samples from the skin penetration study of NBD-PC labeled ethosomes. (A) NBD-PC labeled ethosomes distribution in skin after treated for 24 h. (B). NBD-PC labeled and RhB loaded ethosomes distribution in the skin after treated for 24 h).

was removed and added 2 mL, 20 mg/mL DPH water solution as control. The skin treated with blank ethosomes were divided into three groups. After removing the blank ethosomes, 2 mL, 20 mg/mL DPH water solution was added on the skin at 0 h, 6 h, and 12 h respectively in different group. After adding the DPH water solution to each group, the transdermal receiving solution was taken and the content was determined by high performance liquid phase method (Kim and Gwak, 2011). n = 3 in each group. Specific calculation references 2.5.

4. Results and discussion

4.1. Characterization of ethosomes

The prepared ethosomes had light blue opalescence and the particle size distribution was around 120 nm (Fig. 2C) with polydispersity index (PDI) 0.244 (Table 1). By TEM (Fig. 2B), it could be observed that the ethosomes exhibited vesicular structure. The zeta potential of DPH ethosomes was 25.8 mV (Table 1), which suggested good stability. The encapsulated efficiency (%) of DPH ethosomes was 78.21 ± 0.37 (Table 1). According to the transdermal experiment the transdermal

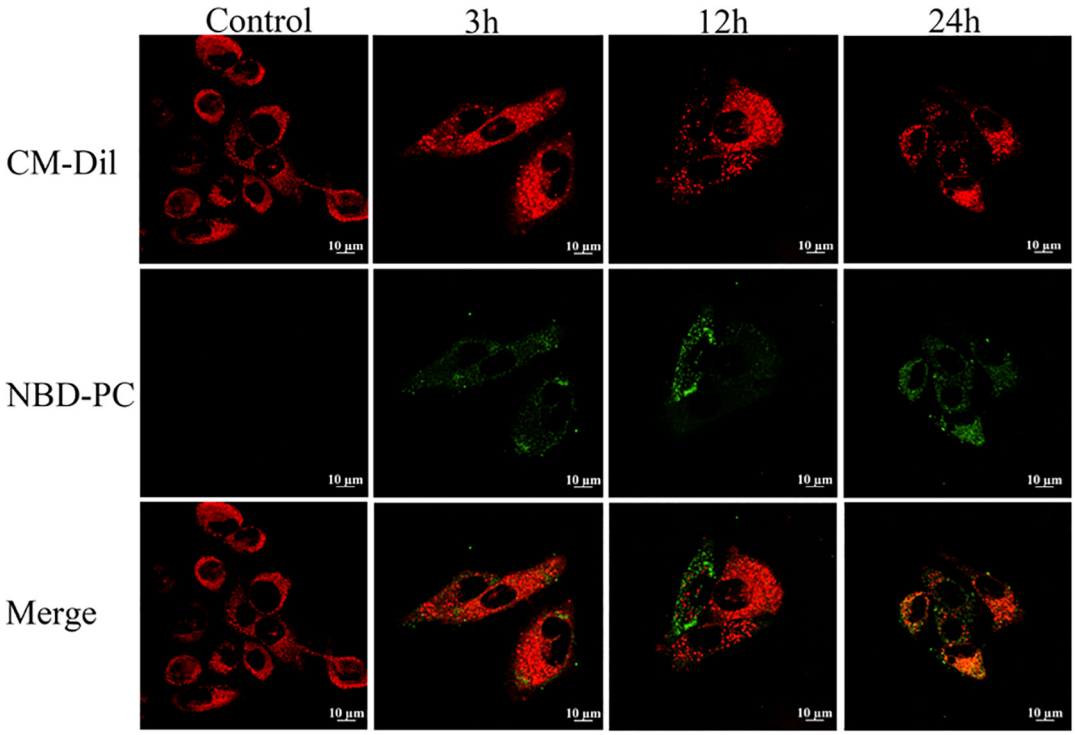

Fig 9. Confocal laser scanning microscopy images of keratinocytes are co-incubated with ethosomes (green stand for ethosomes, red stand for cell membrane).

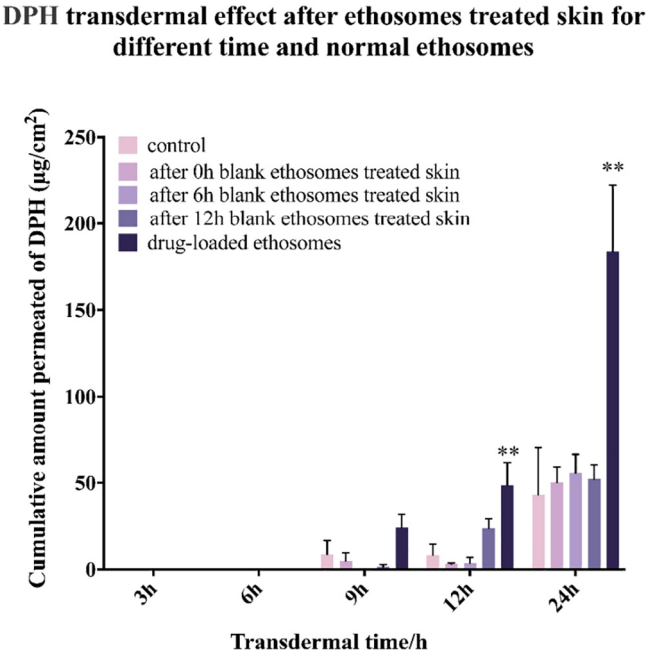

Fig 10. The transdermal effect after ethosomes treated skin for different time and normal ethosomes (n = 3, * denotes statistical significance at a level of $p < 0.05$; ** denotes statistical significance at a level of $p < 0.01$).

amount of DPH in the ethosomes was significantly higher than that in the control group (DPH aqueous solution) and the ethanol solution group at 9 h、12 h and 24 h, demonstrating that ethosomes could significantly promote the DPH penetration in the skin(Fig. 2D and Table S1).

4.2. ATR–FTIR reflects C—H bond changes in the SC

ATR–FTIR is a technique for non-destructive characterizing the SC at the molecular level. The absorption peaks of the main functional groups in the skin were shown in Fig. 3. The following skin bands were obtained from skin intercellular lipids and corneocytes were of interest (Hasanovic et al., 2011): any O—H and N—H stretches from protein, water and lipid were observed between 3000 and 3600 cm^{-1}. CH_2 asymmetric (~2920 cm^{-1}) and symmetric stretching vibration (~2850 cm^{-1}) and CH_2 scissoring vibration (1460 ~ 1470 cm^{-1}) were from SC intercellular lipids. Also, the stretching of lipid ester in SC and amide I (C═O stretching) and amide II (C—N stretching) linkage of the helical secondary structure found in epidermal keratin were presented at about 1640 cm^{-1} and 1540 cm^{-1}. Similarly, C═O stretching band from the fatty acids was at about 1740 cm^{-1}.

It was of great interest to study the CH_2 stretching bands which showed SC lipids change (Obata et al., 2010). Analyses of these bands provided information about conformational order (gauche/trans conformer) of the lipid alkyl chains (Binder et al., 2018). After skin treated by DPH ethosomes, symmetric and asymmetric methylene stretching bands were shifted to significantly higher values compared with the control samples (Table 2), which indicated a lipid order–disorder transition (Fig. 3B). This transition also involved an increase in the fluidity of the SC lipids that could increase the skin penetration of DPH (Bernal-Chavez et al., 2017). Furthermore, after the SC defatting, the absorption intensity of the symmetric and antisymmetric C—H stretching vibration was significantly weakened (Clancy et al., 1994). The treatment with DPH ethosomes and DPH ethanol solution showed significant decrease in symmetric and antisymmetric C—H absorption intensity (Table 2), which has related to the degreasing effect of ethanol.

CH_2 scissoring band displayed a characteristic of the orthorhombic lattice, which was very important for the barrier function of the lipids (Salimi et al., 2016). The spilt of the band was indicative of the degree of inter-chain interaction and the size of the domain with orthorhombic organisation (Kumar et al., 2015). In the spectra of the control group (PBS group), the scissoring width was ~56.57 cm^{-1}, indicating a high content of orthorhombic lattice phase. The treatment with DPH ethosomes showed significant increase of width of the CH_2 scissoring band (Tables 2). In conclusion, the FTIR data suggested that the SC barrier

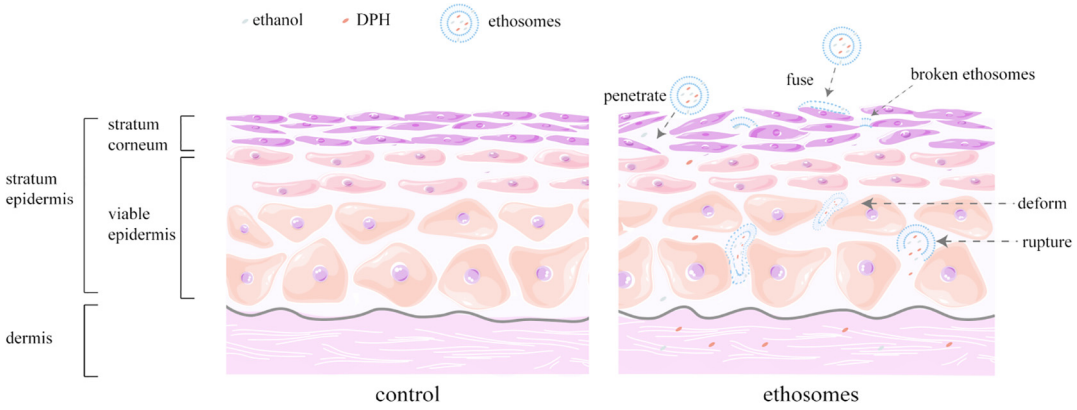

Fig 11. Schematic diagram of ethosomes transdermal mechanism.

function was partially overcomed by DPH ethosomes application.

4.3. Laser confocal Raman reflects C—C bond changes in the SC

Raman spectroscopy and infrared absorption spectroscopy are two largely complementary methods. Raman scattering signals and infrared absorption bands derive from similar types of molecular motions, i.e. bond and lattice vibrations or rotations. However, many molecular modes that yield weak Raman signals show intense infrared absorption and many molecular modes that yield intense Raman signals show weak infrared absorption. The Raman spectrum of the skin was complex (Fig. 4) and some studies have specifically explored the attribution of the peaks (Lopes et al., 2016). At the same time, there was also a report to study the oil effect on phospholipid C—H and C—C in the SC through Raman map changes (Wallach et al., 1979). Therefore, two segments of the feature map were selected for analysis (Fig. 5A and C).

One of the region was C—C stretching (1050–1150 cm^{-1}) and the skeletal optical modes were highly sensitive to hydrocarbon state (Binder et al., 2017). In order to calculate the trans-gauche conformation of skin lipid from viewpoint of the C—C skeleton vibration (Fig. 5B), the value $S_{skeleton} = I_{1080}/(I_{1130} + I_{1060})$ was introduced. I_{1080} was the peak intensity at 1080 cm^{-1}, which resulted from the gauche conformation of the skin (more disordered packing), as well as I_{1130} and I_{1060} were the peak intensities at 1130 cm^{-1} and 1060 cm^{-1}, which corresponded to the all trans conformation of the skin (more ordered packing) (Klossek et al., 2017). Thus, a higher $S_{skeleton}$ value represented a tendency towards a disordered state of skin, while lower values represented a tendency towards a more ordered state of skin (Tfayli et al., 2010) (Fig. 5B). The results showed that after the skin was treated by DPH ethosomes, the $S_{skeleton}$ value was significantly higher than that of the control group (PBS group), which indicated that the skin became more disordered (Fig. 5E).

The other region selected was C—H region. Diverse membranes yield prominent Raman scattering bands in the CH stretching region, due primarily to the CH stretching vibrations of CH_2 and CH_3 residues (Franzen and Windbergs, 2015). In order to obtain further information about the skin lipid C—H vibration conformation order (Choe et al., 2017), the lateral packing order S_{lat} was introduced as $S_{lat} = I_{2880}/I_{2850}$(Fig. 5D). Here, I_{2883} and I_{2847} were the lipid-related Raman peak intensities measured at around 2880 and 2850 cm^{-1}. Symmetric CH_2 stretching vibrations were near 2850 cm^{-1} and the asymmetric vibrations were around 2880 cm^{-1}. A higher S_{lat} represented a more ordered state of skin, while lower S_{lat} represented the more disordered state of skin packing order (Fig. 5D). The results showed that after the skin was treated by DPH ethosomes and DPH ethanol solution, the S_{lat} value was significantly lower than that of the control group (PBS group), which indicated that the SC of the skin changed from an ordered state to a disordered state (Fig. 5E).

In conclusion, the Raman spectrum showed that the C—C bond and the C—H bond of the phospholipid in the skin after contacting ethosomes were unstable. Raman results were consistent with ATR–FTIR results.

4.4. DSC reflects thermodynamic changes of SC

Since DSC technique is widely used to investigate the effect of percutaneous penetration enhancers and retardants on the thermotropic behavior of SC by comparing the endotherms and exotherms for mean transition temperature (T_m) and their enthalpies ($\triangle$H)), it is used to understand the molecular mechanism of each formulation on SC (Esmail et al., 2012). The shift in T_m to lower temperature is interpreted as disruption of the lipid bilayer while reduction in ΔH is ascribed to fluidization of lipid bilayers. Studies have shown that the T_m and $\triangle$H of human skin after treated by lauramide was significantly reduced and skin permeability was increased (Liu et al., 2017). It was worth noting that the T_m of human skin, pig skin, mouse skin and rabbit skin was significantly different (Kaushik and Michniak-Kohn, 2010). DSC of the pig SC produced two endothermic transition peaks at temperatures around 60–70 °C (T_{m1}) and 140–180 °C (T_{m2}). T_{m1} corresponded to the lipid transformation from a lamellar to disordered state. T_{m2} was known to occur due to the irreversible denaturation of proteins in the SC (Brandwein et al., 2018). Therefore, we mainly focused on T_{m1} to understand lipid transformation in this study (Fig. 6A).

Ethosomes and 30% ethanol solution treated skin samples significantly reduced their T_m values (Fig. 6B and C) and $\triangle$H (Fig. 6D), when compared to the other treatments ($p < 0.05$), which indicated that these formulations had a more significant effect on fluidization and disruption of skin lipid bilayers. It was precisely because the fluidity of the phospholipids in the skin increases, which made the formulation easier to penetrate the skin barrier.

4.5. SEM and TEM reflects ultrastructure of the SC

Fig. 7A–H showed images of the skin surface treated with the control, DPH water solution, DPH ethosomes and 30% ethanol DPH solution for 24 h, respectively.

Macroscopical observations of the skin treated with different formulations were operated by SEM. SEM has a large depth of field compared with conventional light microscopy and for that reason the images obtained have a three-dimensional appearance, high resolution at high magnifications, revealing details of the skin surface (Zhang et al., 2015). Related studies have used SEM to observe effect of the transdermal penetration enhancer menthol and menthone on the SC (Wang et al., 2017). The details of the skin structure with different layers, such as the desquamation of the skin, could be seen (Sapra et al., 2009). The SC was composed of corneocytes enclosed by a continuous

intercellular lipid domain. The important differences among these images were the extent of SC exfoliation, which corresponded to the corneocytes after the lipid extraction by penetration enhancers (Sapra et al., 2009). It was observed that a large number of pieces were desquamated from the porcine skin treated by DPH ethosomes and DPH ethanol (Fig. 7C and D) while there was almost no desquamated SC piece in the PBS and DPH water solution treated skin (Fig. 7A and B). Therefore, when the porcine skin was dipped in the ethosomes and 30% ethanol DPH solution enhancer solution, the intercellular lipid could be dissolved and extracted, leading to the separation and desquamation from intact SC, which could cause the skin permeability to increase. Furthermore, the desquamated extent could reflect the ability of formulations to extract lipids.

TEM is the most efficient way to visualize the ultrastructure of the SC (Bhatia et al., 1997; Bhatia and Singh, 1999; Sapra et al., 2008). The ultrastructure of pig skin treated by different formulations was showed in Fig. 7E–H. Closely packed SC cells layers and a tightly packed keratin pattern was observed in the control epidermis (Fig. 7E and F). Treatment of epidermis with 30% ethanol solution resulted in the loss of intercellular material, a disruption of keratin pattern, and further swelling of SC cell layers (Fig. 7H). Also, the intercellular space between the SC cells was increased, which indicated the increase free volume. However, treatment of the SC with ethosomes did not result in swelling of SC cell layers and a disruption of keratin pattern (Fig. 7G), which meant ethosomes did not cause irreversible damage to the pig skin. The ultrastructure of the skin after treatment with ethosomes and ethanol was clearly different, indicating that their mechanism of action was different.

4.6. Fluorescence labeling shows ethosomes distribution in the pig skin

In order to study the distribution of ethosomes in the skin, fluorophores were directly connected with phospholipids by chemically bonding to avoid physical adsorption shedding. Thus, NBD-PC (Brewer et al., 2013) was used as a tracer of phospholipids to prepare fluorescent ethosomes. At the same time, RhB was used to further explore the mechanism. Due to the presence of autofluorescence in the skin, it was necessary to adjust appropriate imaging conditions to avoid autofluorescence interference. No fluorescence was observed in the control group (PBS group) (Fig. 8A), which indicated that autofluorescence interference in the skin has been avoided. And ethosomes were mainly distributed in the SC and the depth of entry was about 30 μm (Fig. 8A). The existence of green fluorescence- NBD-PC labeled phospholipids in the dermis was not found. Furthermore, NBD-PC fluorescence was mainly distributed in the intercellular space at about 10 μm under the top SC, which suggested that the ethosomes penetrated the skin mainly through the intercellular pathway after penetrating the upper SC.

In addition, NBD-PC labled ethosomes carring RhB distribution in skin was also studied. From the Fig. 8B, the fluorescence intensity of solution group was weaker than that of ethosomes group, indicating that ethosomes significantly promoted the transdermal of RhB. Furthermore, the green fluorescence of NBD-PC remained in the viable epidermis at 24 h while a broader distribution of red fluorescence of RhB was seen in the dermis or deep layer of the skin without green fluorescence of NBD-PC, which suggested that the distribution difference between the two fluorescent compounds emerged. This difference reminded that ethosomes experienced sphere separation and drug release in the superficial epidermis. Noteworthy, the distribution of RhB and NBD-PC were centralized in the gap between skin cells. To further determine this phenomenon, the experiment at cell level was carried out.

4.7. Cell study to explore the interaction between ethosomes and keratinocyte

First, the cell membrane of keratinocytes was labeled by CM-Dil with red fluorescence, and then co-incubated with green fluorescence labeled ethosomes. With the increase of time, the green fluorescence intensity of the ethosome increased on the cell membrane (Fig. 9). But it was basically distributed on the cell membrane, and the fluorescence intensity inside the cell was basically undetectable. This showed that the ethosomes were mainly through the intercellular space during the active SC transdermal process from the cellular level, which was consistent with the results of the skin section.

4.8. Blank ethosomes pre-treatment of skin does not promote DPH transdermal penetration

Finally, based on the above research, the blank ethosomes was used to treat the skin for 24 h, and then added drugs to determine whether the carrier of the ethosomes was necessary for drug penetration. After the skin treated by the blank ethosomes, the DPH solution was added to the skin at 0 h, 6 h, and 12 h. The transdermal amount of DPH was not significantly different from the control group (DPH aqueous solution) (Fig. 10 and Table S2). However, the transdermal amount of DPH loaded by ethosomes was significantly higher than the control group (DPH aqueous solution). This indicated that transdermal delivery of DPH must be carried by ethosomes and blank ethosomes pre-treatment of skin did not promote transdermal penetration of DPH.

5. Conclusion

Based on our results from this study, it was concluded that both ethosomes and ethanol solution could disturb lipid domain of SC, dissolve and extract the intercellular lipid, as well as change the transition temperature of SC. Therefore, it could enhance the fluidity of the SC and allow drug to penetrate easily into deeper layers of the skin. The difference was that the ethanol solution made SC swell and keratinous space increase, while the ethosomes did not have such effect. While, the transdermal permeation effect of the ethosomes was significantly better than that of the ethanol solution. It was largely due to the ethosomes carrying the drug to penetrate skin against the SC barrier. It was worth noting that a part of the ethosomes were fused with the upper SC. And the other part of ethosomes went through the intercellular space and ruptured to release the drug during penetrating SC, which allowed drugs to permeate into the deeper layer alone (Fig. 11).

Declaration of Competing Interest

The authors declare that they have no known competing financial interests or personal relationships that could have appeared to influence the work reported in this paper.

Acknowledgment

This study was partly supported by National Key R&D Program of China (No. 2017YFE0102200), National Natural Science Foundation of China (81872213) and National Natural Science Foundation of Zhejiang Province (LY17H310002).

Appendix A. Supplementary data

Supplementary data to this article can be found online at https://doi.org/10.1016/j.ijpx.2019.100027.

References

Abd El-Alim, S.H., Kassem, A.A., Basha, M., Salama, A., 2019. Comparative study of liposomes, ethosomes and transfersomes as carriers for enhancing the transdermal delivery of diflunisal: in vitro and in vivo evaluation. Int. J. Pharm. 563, 293–303.
Ashtikar, M., Nagarsekar, K., Fahr, A., 2016. Transdermal delivery from liposomal formulations – evolution of the technology over the last three decades. J. Controlled Release 242, 126–140.

Bernal-Chavez, S.A., Perez-Carreto, L.Y., Nava-Arzaluz, M.G., Ganem-Rondero, A., 2017. Alkylglycerol derivatives, a new class of skin penetration modulators. Molecules 22, 185–196.
Bhatia, K.S., Gao, S., Singh, J., 1997. Effect of penetration enhancers and iontophoresis on the FT-IR spectroscopy and LHRH permeability through porcine skin. J. Controlled Release 47, 81–89.
Bhatia, K.S., Singh, J., 1999. Effect of linolenic acid/ethanol or limonene/ethanol and iontophoresis on the in vitro percutaneous absorption of LHRH and ultrastructure of human epidermis. Int. J. Pharm. 180, 235–250.
Binder, L., SheikhRezaei, S., Baierl, A., Gruber, L., Wolzt, M., Valenta, C., 2017. Confocal Raman spectroscopy: in vivo measurement of physiological skin parameters – a pilot study. J. Dermatol. Sci. 88, 280–288.
Binder, L., Kulovits, E.M., Petz, R., Ruthofer, J., Baurecht, D., Klang, V., Valenta, C., 2018. Penetration monitoring of drugs and additives by ATR-FTIR spectroscopy/tape stripping and confocal Raman spectroscopy – a comparative study. Eur. J. Pharm. Biopharm. 130, 214–223.
Bouwstra, J.A., Ponec, M., 2006. The skin barrier in healthy and diseased state. BBA 1758, 2080–2095.
Brandwein, M., Fuks, G., Israel, A., Al-Ashhab, A., Nejman, D., Straussman, R., Hodak, E., Harari, M., Steinberg, D., Bentwich, Z., Shental, N., Meshner, S., 2018. Temporal stability of the healthy human skin microbiome following dead sea climatotherapy. Acta Derm. Venereol. 98, 256–261.
Brewer, J., Bloksgaard, M., Kubiak, J., Sorensen, J.A., Bagatolli, L.A., 2013. Spatially resolved two-color diffusion measurements in human skin applied to transdermal liposome penetration. J. Invest. Dermatol. 133, 1260–1268.
Cevc, G., Vierl, U., 2010. Nanotechnology and the transdermal route: a state of the art review and critical appraisal. J. Controlled Release 141, 277–299.
Chen, Z.X., Li, B., Liu, T., Wang, X., Zhu, Y., Wang, L., Wang, X.H., Niu, X., Xiao, Y., Sun, Q., 2017. Evaluation of paeonol-loaded transethosomes as transdermal delivery carriers. Eur. J. Pharm. Sci. 99, 240–245.
Choe, C., Schleusener, J., Lademann, J., Darvin, M.E., 2017. In vivo confocal Raman microscopic determination of depth profiles of the stratum corneum lipid organization influenced by application of various oils. J. Dermatol. Sci. 87, 183–191.
Clancy, M.J., Corish, J., Corrigan, O.I., 1994. A comparison of the effects of electrical-current and penetration enhancers on the properties of human skin using spectroscopic (Ftir) and calorimetric (Dsc) methods. Int. J. Pharm. 105, 47–56.
Esmail, H., Barry 3rd, C.E., Wilkinson, R.J., 2012. Understanding latent tuberculosis: the key to improved diagnostic and novel treatment strategies. Drug Discov. Today 17, 514–521.
Fan, C., Li, X., Zhou, Y., Zhao, Y., Ma, S., Li, W., Liu, Y., Li, G., 2013. Enhanced topical delivery of tetrandrine by ethosomes for treatment of arthritis. Biomed. Res. Int. 16, 1943–1951.
Franzen, L., Windbergs, M., 2015. Applications of Raman spectroscopy in skin research–from skin physiology and diagnosis up to risk assessment and dermal drug delivery. Adv. Drug Deliv. Rev. 89, 91–104.
Goindi, S., Dhatt, B., Kaur, A., 2014. Ethosomes-based topical delivery system of antihistaminic drug for treatment of skin allergies. J. Microencapsul. 31, 716–724.
Hasanovic, A., Winkler, R., Resch, G.P., Valenta, C., 2011. Modification of the conformational skin structure by treatment with liposomal formulations and its correlation to the penetration depth of aciclovir. Eur. J. Pharm. Biopharm. 79, 76–81.
Kaushik, D., Michniak-Kohn, B., 2010. Percutaneous penetration modifiers and formulation effects: thermal and spectral analyses. AAPS PharmSciTech 11, 1068–1083.
Kim, K.H., Gwak, H.S., 2011. Effects of vehicles on the percutaneous absorption of donepezil hydrochloride across the excised hairless mouse skin. Drug Dev. Ind. Pharm. 37, 1125–1130.
Klossek, A., Thierbach, S., Rancan, F., Vogt, A., Blume-Peytavi, U., Ruhl, E., 2017. Studies for improved understanding of lipid distributions in human skin by combining stimulated and spontaneous Raman microscopy. Eur. J. Pharm. Biopharm. 116, 76–84.
Kumar, S., Zakrewsky, M., Chen, M., Menegatti, S., Muraski, J.A., Mitragotri, S., 2015. Peptides as skin penetration enhancers: mechanisms of action. J. Controlled Release 199, 168–178.
Lam, P.L., Gambari, R., 2014. Advanced progress of microencapsulation technologies: in vivo and in vitro models for studying oral and transdermal drug deliveries. J. Controlled Release 178, 25–45.
Li, N., Peng, L.H., Chen, X., Zhang, T.Y., Shao, G.F., Liang, W.Q., Gao, J.Q., 2014. Antigen-loaded nanocarriers enhance the migration of stimulated Langerhans cells to draining lymph nodes and induce effective transcutaneous immunization. Nanomedicine 10, 215–223.
Limsuwan, T., Boonme, P., Khongkow, P., Amnuaikit, T., 2017. Ethosomes of phenylethyl resorcinol as vesicular delivery system for skin lightening applications. Biomed. Res. Int. 2017, 19–31.
Liu, W.H., Teng, L.R., Yu, K.T., Sun, X.S., Fan, C.Y., Long, C.X., Liu, N., Li, S., Wu, B., Xu, Q.J., Sun, F.Y., Li, Y.X., 2017. Design of hydrogels of 5-hydroxymethyl tolterodine and their studies on pharmacokinetics, pharmacodynamics and transdermal mechanism. Eur. J. Pharm. Sci. 96, 530–541.
Lopes, J., Correia, M., Martins, I., Henriques, A.G., Delgadillo, I., Silva, O.D.E., Nunes, A., 2016. FTIR and Raman spectroscopy applied to dementia diagnosis through analysis of biological fluids. J. Alzheimers Dis. 52, 801–812.
Mandal, B., Rameshbabu, A.P., Soni, S.R., Ghosh, A., Dhara, S., Pal, S., 2017. In situ silver nanowire deposited cross-linked carboxymethyl cellulose: a potential transdermal anticancer drug carrier. ACS Appl. Mater. Interfaces 9, 36583–36595.
Marto, J., Vitor, C., Guerreiro, A., Severino, C., Eleuterio, C., Ascenso, A., Simoes, S., 2016. Ethosomes for enhanced skin delivery of griseofulvin. Colloids Surf. B Biointerfaces 146, 616–623.
Melot, M., Pudney, P.D.A., Williamson, A.M., Caspers, P.J., Van Der Pol, A., Puppels, G.J., 2009. Studying the effectiveness of penetration enhancers to deliver retinol through the stratum cornum by in vivo confocal Raman spectroscopy. J. Controlled Release 138, 32–39.
Moll, K.P., Herrmann, W., Stosser, R., Borchert, H.H., 2008. Changes of the properties in the upper layers of human skin on treatment with models of different pharmaceutical formulations – an ex vivo ESR imaging study. ChemMedChem 3, 653–659.
Obata, Y., Utsumi, S., Watanabe, H., Suda, M., Tokudome, Y., Otsuka, M., Takayama, K., 2010. Infrared spectroscopic study of lipid interaction in stratum corneum treated with transdermal absorption enhancers. Int. J. Pharm. 389, 18–23.
Oh, S.Y., Fujii, M., Takeda, Y., Yoda, K., Utoguchi, N., Matsumoto, M., Watanabe, Y., 2002. The effect of ethanol on the simultaneous transport and metabolism of methyl p-hydroxybenzoate in excised skin of Yucatan micropig. Int. J. Pharm. 236, 35–42.
Park, S.H., Shin, H.S., Park, S.N., 2018. A novel pH-responsive hydrogel based on carboxymethyl cellulose/2-hydroxyethyl acrylate for transdermal delivery of naringenin. Carbohydr. Polym. 200, 341–352.
Polat, B.E., Deen, W.M., Langer, R., Blankschtein, D., 2012. A physical mechanism to explain the delivery of chemical penetration enhancers into skin during transdermal sonophoresis – Insight into the observed synergism. J. Controlled Release 158, 250–260.
Rao, Y.F., Zheng, F.Y., Zhang, X.G., Gao, J.Q., Liang, W.Q., 2008. In vitro percutaneous permeation and skin accumulation of finasteride using vesicular ethosomal carriers. Aaps Pharmscitech 9, 860–865.
Roberts, M.S., Mohammed, Y., Pastore, M.N., Namjoshi, S., Yousef, S., Alinaghi, A., Haridass, I.N., Abd, E., Leite-Silva, V.R., Benson, H.A.E., Grice, J.E., 2017. Topical and cutaneous delivery using nanosystems. J. Controlled Release 247, 86–105.
Salimi, A., Hedayatipour, N., Moghimipour, E., 2016. The effect of various vehicles on the naproxen permeability through rat skin: a mechanistic study by DSC and FT-IR techniques. Adv. Pharm. Bull. 6, 9–16.
Saluja, S., Kasha, P.C., Paturi, J., Anderson, C., Morris, R., Banga, A.K., 2013. A novel electronic skin patch for delivery and pharmacokinetic evaluation of donepezil following transdermal iontophoresis. Int. J. Pharm. 453, 395–399.
Sapra, B., Jain, S., Tiwary, A.K., 2008. Transdermal delivery of carvedilol containing glycyrrhizin and chitosan as permeation enhancers: biochemical, biophysical, microscopic and pharmacodynamic evaluation. Drug Deliv. 15, 443–454.
Sapra, B., Jain, S., Tiwary, A.K., 2009. Effect of Asparagus racemosus extract on transdermal delivery of carvedilol: a mechanistic study. AAPS PharmSciTech 10, 199–210.
Schmidt, R., Hofer, E., Bouwman, F.H., Buerger, K., Cordonnier, C., Fladby, T., Galimberti, D., Georges, J., Heneka, M.T., Hort, J., Laczo, J., Molinuevo, J.L., O'Brien, J.T., Religa, D., Scheltens, P., Schott, J.M., Sorbi, S., 2015. EFNS-ENS/EAN Guideline on concomitant use of cholinesterase inhibitors and memantine in moderate to severe Alzheimer's disease. Eur. J. Neurol. 22, 889–898.
Tfayli, A., Guillard, E., Manfait, M., Baillet-Guffroy, A., 2010. Thermal dependence of Raman descriptors of ceramides. Part I: effect of double bonds in hydrocarbon chains. Anal. Bioanal. Chem. 397, 1281–1296.
Touitou, E., Dayan, N., Bergelson, L., Godin, B., Eliaz, M., 2000. Ethosomes – novel vesicular carriers for enhanced delivery: characterization and skin penetration properties. J. Controlled Release 65, 403–418.
Wallach, D.F., Verma, S.P., Fookson, J., 1979. Application of laser Raman and infrared spectroscopy to the analysis of membrane structure. Biochim. Biophys. Acta 559, 153–208.
Wang, J.Y., Dong, C.L., Song, Z.J., Zhang, W.J., He, X., Zhang, R.Q., Guo, C.R., Zhang, C.F., Li, F., Wang, C.Z., Yuan, C.S., 2017. Monocyclic monoterpenes as penetration enhancers of ligustrazine hydrochloride for dermal delivery. Pharm. Dev. Technol. 22, 571–577.
Wang, C., Zhu, J., Zhang, D., Yang, Y., Zheng, L., Qu, Y., Yang, X., Cui, X., 2018. Ionic liquid - microemulsions assisting in the transdermal delivery of Dencichine: preparation, in-vitro and in-vivo evaluations, and investigation of the permeation mechanism. Int. J. Pharm. 535, 120–131.
Yang, L., Wu, L., Wu, D., Shi, D., Wang, T., Zhu, X., 2017. Mechanism of transdermal permeation promotion of lipophilic drugs by ethosomes. Int. J. Nanomed. 12, 3357–3364.
Yang, H.J., Wu, X.J., Zhou, Z.Z., Chen, X.G., Kong, M., 2019. Enhanced transdermal lymphatic delivery of doxorubicin via hyaluronic acid based transfersomes/microneedle complex for tumor metastasis therapy. Int. J. Biol. Macromol. 125, 9–16.
Yin, Q., Wang, R., Yang, S., Wu, Z., Guo, S., Dai, X., Qiao, Y., Shi, X., 2017. Influence of temperature on transdermal penetration enhancing mechanism of borneol: a multi-scale study. Int. J. Mol. Sci. 18, 195–206.
Yu, X., Du, L., Li, Y., Fu, G., Jin, Y., 2015. Improved anti-melanoma effect of a transdermal mitoxantrone ethosome gel. Biomed. Pharmacother. 73, 6–11.
Zhang, Y.T., Shen, L.I.N., Zhao, J.H., Feng, N.P., 2014. Evaluation of psoralen ethosomes for topical delivery in rats by using in vivo microdialysis. Int. J. Nanomed. 9, 669–678.
Zhang, W.J., Wang, J.Y., Li, H., He, X., Zhang, R.Q., Zhang, C.F., Li, F., Yang, Z.L., Wang, C.Z., Yuan, C.S., 2015. Novel application of natural anisole compounds as enhancers for transdermal delivery of ligustrazine. Am. J. Chin. Med. 43, 1231–1246.
Zhao, H., Liu, C., Quan, P., Wan, X., Shen, M., Fang, L., 2017. Mechanism study on ion-pair complexes controlling skin permeability: effect of ion-pair dissociation in the viable epidermis on transdermal permeation of bisoprolol. Int. J. Pharm. 532, 29–36.